INTERNATIONAL JOURNAL FOR NUMERICAL METHODS IN FLUIDS
Int. J. Numer. Meth. Fluids 2005; **47**:1115–1122
Published online 21 January 2005 in Wiley InterScience (www.interscience.wiley.com). DOI: 10.1002/fld.878

Reduced basis simulations as a tool for generating turbulent inlet-data for two opposing jets

Peter S. Johansson[‡] and Helge I. Andersson[*,†]

Department of Energy and Process Engineering, Norwegian University of Science and Technology, 7491 Trondheim, Norway

SUMMARY

Reduced basis simulations are used in order to generate turbulent inlet boundary conditions for a direct numerical simulation of two opposing wall jets. The two entering jets are fully turbulent channel flows of Reynolds number 180, based on friction velocity and half channel height. The inflow turbulence is generated by solving dynamical equations for the large scales only, while less energetic small scales are added randomly. The proper orthogonal decomposition method is used to identify the large scale modes used in the basis set. Mean velocity and turbulence statistics have been reported in various planes of the interaction region and the outwash jet. The increase in maximum turbulence energy from the inlet jet to the stagnation region is about 500%. The spreading rate of the merged jet was found to be 0.125.

KEY WORDS: low dimensional dynamical systems; inflow generation; DNS; fountain flow; jet flow

1. BACKGROUND AND METHOD

Two opposing turbulent jets interacting in the presence of a wall (see Figure 1) are investigated by means of direct numerical simulations (DNS). The stagnation flow is similar to the fountain flow which is set up when a fighter plane's twin jet is directed downwards to hold the plane still in the air [1], or the flow in chemical reactors where two opposing jets are used in order to enhance the mixing [2]. The flow has strong dynamics and is different from shear flows in which the mean shear is the heart of the turbulence production. In stagnation flows, the mean rate of normal strain is important and there is considerable streamline curvature which results in other turbulence transport and production mechanisms than those found in pure shear flows. The turbulence in such flows has been shown awkward to accurately model [3].

*Correspondence to: Helge I. Andersson, Department of Energy and Process Engineering, Norwegian University of Science and Technology, 7491 Trondheim, Norway.
†E-mail: helge.i.andersson@ntnu.no
‡E-mail: peter.s.johansson@ntnu.no

Received 27 April 2004
Revised 1 September 2004
Accepted 22 September 2004

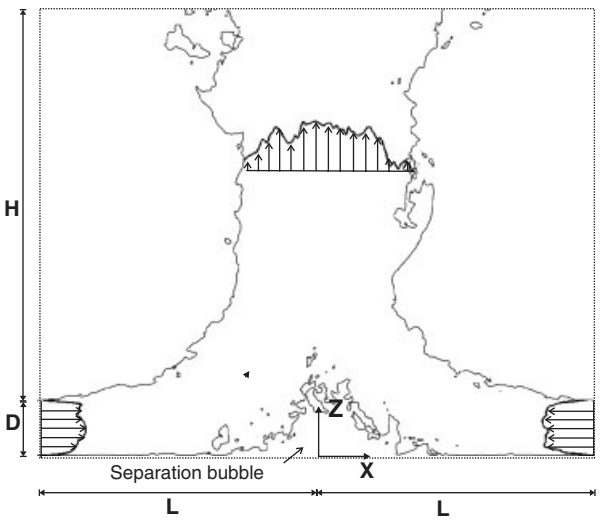

Figure 1. Sketch of flow geometry.

Experimental studies of the outwash flow arising from two colliding turbulent jets show very high turbulence intensities in the stagnation region [4, 5]. Another interesting feature is that the fountain jet has growth rates considerably larger than the growth rates found in free planar jets [6].

In numerical simulations of turbulent flows, there are mainly three aspects that determine the accuracy of the simulation: the applied numerical method, the adopted turbulence model and the prescribed boundary conditions and especially those at the inflow boundary. Inaccurate inflow boundary conditions can seriously influence the simulation results [7, 8].

The turbulent flow field at the open boundary needs to have spatial and temporal variations, and the incoming velocity field should have a correct mean value, fulfil the incompressibility constraint, have proper one- and two-point correlations and ultimately meet the momentum equation. See Reference [9] for a short and recent review on different inflow generation methods. The most realistic turbulent inflow is generally achieved by performing an auxiliary simulation which typically uses periodic boundary conditions. However, such a simulation puts extra demands on the computational resources.

In the present study, two fully turbulent plane channel flows of Reynolds number 180, based on friction velocity and half channel height, enter from either sides of the domain. The inflow boundary conditions mimicking these two turbulent jets are produced by two reduced simulations based on a selected set of the most energetic modes from a proper orthogonal decomposition (POD) of a previously performed DNS of plane channel flow.

The proper orthogonal decomposition [10] is a statistical method used to identify which degrees of freedom are the most active or energetic in a stochastic process, which in this case is a turbulent flow field. These modes or structures constitute a set of orthogonal basis functions which are optimal (in comparison with any other linear basis) in terms of representing the energy of the velocity fields from which the POD-modes are derived. Other favourable qualities of the modes are that they fulfil the incompressibility constraint and the same boundary conditions as the velocity field.

For the plane channel flow, which is statistically homogeneous in the x- and y-direction, the POD modes are of the form

$$\boldsymbol{\varphi}^q_{mn}(\boldsymbol{x}) = \boldsymbol{\phi}^q_{mn}(z)\mathrm{e}^{2\pi\mathrm{i}(mx/L_x + ny/L_y)} \tag{1}$$

in which m and n are the number of periods in the x- and y-direction and q is the vertical quantum number indexing various wall-normal expansions. The velocity field at time t_s can be expressed as

$$\boldsymbol{u}(\boldsymbol{x}, t_s) = \sum_{mnq} a^q_{mn}(t_s)\boldsymbol{\varphi}^q_{mn}(\boldsymbol{x}) \tag{2}$$

in which $\boldsymbol{\varphi}^q_{mn}(\boldsymbol{x})$ are the spatial basis functions and $a^q_{mn}(t_s) = \int \boldsymbol{u}(\boldsymbol{x}, t_s) \cdot \boldsymbol{\varphi}(\boldsymbol{x})^{q*}_{mn}\,\mathrm{d}\boldsymbol{x}$ are the associated coefficients.

The dynamical system prescribing the temporal behaviour of the coefficients $a^q_{mn}(t)$ is derived by Galerkin projecting the Navier–Stokes equations on to the POD basis. In this way, the large-scale motion produced by the dynamical system is a linear expansion of structures present in the real flow (DNS). The basis functions comply with incompressibility which makes the fluctuating pressure cancel out in the Galerkin projection and enables the set of dynamical equations to be advanced in time without having to solve any Poisson equation for the fluctuating pressure. The reduced basis set $\mathscr{S}$ for the present inflow generation corresponds to the quantum numbers Ω: $m = \pm 1, \ldots, \pm M_c$, $n = \pm 1, \ldots, \pm N_c$ and $q = 1, \ldots, Q_c$. When m and n equal 0, $q = 1, \ldots, Q_{c,00}$. In the simulations used here, $M_c = 2$, $N_c = 12$, $Q_c = 10$ and $Q_{c,00} = 32$. The computational domain of the reduced channel simulation measures 6.28, 6.3, and 2 dimensionless length units (see next section on how variables are normalized) in the x-, y- and z-direction, respectively. Less energetic modes, which are not included in the basis, are randomly superimposed in order to have some energy in the small scales. These modes are essential in order to hinder excessive growth of the large scales downstream of the inlet [9]. The amplitudes of the modes, which are added randomly, are generated by a random-number-generator with the distribution

$$f(\alpha) = \begin{cases} 0 & \alpha < 0 \\ \dfrac{2}{\sqrt{2\pi}}\, e^{-\frac{\alpha^2}{2}} & \alpha \geqslant 0 \end{cases} \tag{3}$$

In order to impose some correlation with the preceding time-step we set $\alpha^{\mathrm{new}} = (\alpha^{\mathrm{new}'} + \alpha^{\mathrm{old}})/2$, where $\alpha^{\mathrm{new}'}$ is the random number generated at the present time-step. The amplitudes are then set as $|a^q_{mn}| = \alpha^{\mathrm{new}}\sqrt{\lambda^q_{m,n}}$, where λ^q_{mn} is estimated from the POD of the channel flow.

The phases of temporal coefficients with non-zero streamwise wave-number behave as $\theta_0 + \omega t$, where $\omega = -2\pi m U_{\mathrm{bulk}}/L_{x,\mathrm{red.sim.}}$ in order to imitate the propagating behaviour of these modes [11]. The initial values θ_0 of the phases are set randomly.

The method has been validated in Reference [9] for a DNS and a LES of plane channel flows of different Reynolds numbers. In Figure 2, the turbulent root-mean-square (rms) and shear-stress profiles downstream of a plane channel with generated velocities at the inlet are shown. Statistical quantities such as mean velocities, turbulence intensities, energy spectra and wall friction soon approach the fully developed level and deviate less than 5% from the fully developed state, even very close to the inlet.

For comparisons, results where all modes are varied randomly are also shown in Figure 2. In order to avoid much too rapid temporal variation of the large scales, a more realistic temporal

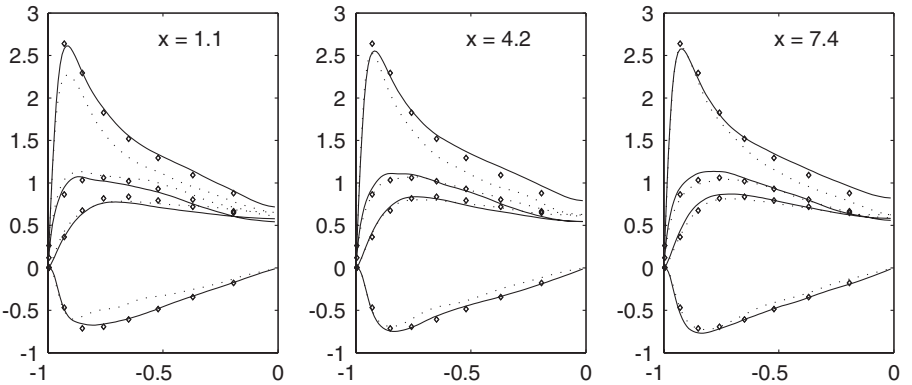

Figure 2. Turbulence intensities and turbulent shear stress downstream of a plane channel with generated inlet velocities [9]. — dynamic and random inflow, · · · fully random inflow. Symbols, DNS of fully developed channel flow.

correlation is used, namely $\alpha^{\text{new}} = (\alpha^{\text{old}} + \sigma\, \mathrm{d}t\, \alpha^{\text{new}'})/(1 + \sigma\, \mathrm{d}t)$. Here, $\mathrm{d}t$ is the time-step and $\sigma = \max(m, n, q)$, where m, n and q are defined in (1).

The fully random generation also gives surprisingly good results downstream of the inlet, even though the streamwise component and shear-stress correlation show some decay at $x = 1.1$. It is believed that the fully random inflow generation method used here is near optimal compared to other fully random methods since a lot of information from the Navier–Stokes equations is incorporated in the POD modes. For the fully random generation, problems are likely to appear if either the channel aspect ratio or Reynolds number is changed from those corresponding to the flow from which the POD modes are extracted. The reduced basis simulations, however, are amenable to at least 50% increase in Reynolds number or aspect ratios of the channel [12].

For the present case, the dynamical system predicting the large scale fluctuating motion has 1272 degrees of freedom (i.e. real differential equations) while about 10^5 modes representing low energetic small scales are added randomly at each time-step. Approximately 30 min on a single 1.2 Gflops processor were used in order to generate 45 dimensionless time units of turbulent channel flow. In this particular case, the computational work of integrating the dynamical system and adding random modes is approximately the same. In order to generate the inflow by performing a full DNS simulation, the in-house finite volume code would require in the order of 10^2 longer time using a single processor and the direct solver.

2. GOVERNING EQUATIONS, BOUNDARY CONDITIONS AND GRID

The incompressible Navier–Stokes equations describing the dynamics of the flow are

$$\frac{\partial \boldsymbol{U}}{\partial t} + \boldsymbol{U} \cdot \nabla \boldsymbol{U} = -\nabla P + \frac{1}{R_*} \nabla^2 \boldsymbol{U} \tag{4}$$

$$\nabla \cdot \boldsymbol{U} = 0 \tag{5}$$

in which the velocity $\boldsymbol{U}=(U,V,W)=(\tilde{U},\tilde{V},\tilde{W})/u_*$, the time $t=2\tilde{t}u_*/\tilde{D}$, the pressure $P=\tilde{P}/(\tilde{\rho}u_*^2)$, the position $\boldsymbol{x}=(x,y,z)=2(\tilde{x},\tilde{y},\tilde{z})/\tilde{D}$ and the Reynolds number $R_*=u_*\tilde{D}/(2\nu)$. The tilde $\tilde{}$ indicates dimensional quantities, u_* is the friction velocity of the channel flow, $\tilde{D}$ is the inlet-channel height and ν is the kinematic viscosity.

The equations are discretized using a finite volume method approach on a staggered grid arrangement [13]. The accuracy in space is of second-order. A fractional step method with an explicit second-order Adams–Bashforth scheme is used in order to impose the continuity constraint while advancing in time.

The pressure gradient is put to zero at the 'channel boundary' where the velocities are given by the inflow generator. At the wall, the usual no-slip boundary condition is specified. In the spanwise direction, periodic boundary conditions are used. The pressure on the open boundary is set to zero. On the left and right open boundary, normal gradients of the velocities are set to zero while on the top boundary convective boundary conditions [14] are used. Tangential velocities are set to zero if there is entrainment of fluid, i.e. inwards normal velocity, on the open boundary in order to mimic quiet surroundings. On the open boundary, the normalized entrainment velocity is not allowed to be larger than 1.

The computational domain has length $2L=20$, width 6.3 and height $D+H=16$. The length in x-direction $2L$ is chosen sufficiently large such that the incoming jets do not experience an adverse pressure gradient when entering the domain. The spanwise width is set such that two-point correlations satisfactorily approach zero within a separation of half the spanwise width. The height of the domain was put equal to 16 and was limited by available computational resources. In total, $448\times192\times448$ grid points are used in the x-, y- and z-direction, respectively. The grid is equidistant in the spanwise y-direction. In the wall normal z-direction the grid is stretched. The first pressure point is placed 0.9 wall units ($z^+=\tilde{z}u_*/\nu$) from the wall. From here, constant stretching of 1% is used until $z=2$ where $\Delta z^+=5.1$. From there to the top boundary, the grid is further stretched. In x-direction, the grid is equidistant in the centre region $-3.7\leqslant x\leqslant3.7$ and here the grid spacing is 5.9 wall units. From $x=\pm3.7$ to the left/right boundary, constant stretching is used.

In order to check if this grid resolution was sufficient, a second simulation was performed on the same computational domain, but with $288\times128\times288$ grid points in the x-, y- and z-direction, respectively. This amounts to approximately one-fourth of the number of grid points used in the fine simulation. Since the mean velocities and the rms-profiles from the two simulations are nearly identical, it is believed that the fine grid resolution is adequate.

The flow configuration is invariant under reflection across the yz-plane and the xz-plane, 180° rotation about the z-axis and translation in y-direction. All variables presented here are averaged over these symmetries as well as in time. This average is denoted by $\langle\,\rangle$. In total, 1350 velocity samples were gathered over 27 dimensionless time units.

3. RESULTS AND CONCLUDING REMARKS

In Figure 3(a)–(c) the mean velocities $\langle U\rangle$ and $\langle W\rangle$ and the mean pressure $\langle P\rangle$ are reported. The channel flow enters at $x=-10$, meets the stagnation pressure and is redirected into the z-direction where it unites with the counter flowing jet. Immediately after the inlet, there is a negative pressure gradient typical to channel flow, but at $x\approx\pm9.5$ a very strong adverse pressure gradient begins. The wall friction (Figure 3(a)) is rapidly reduced and at

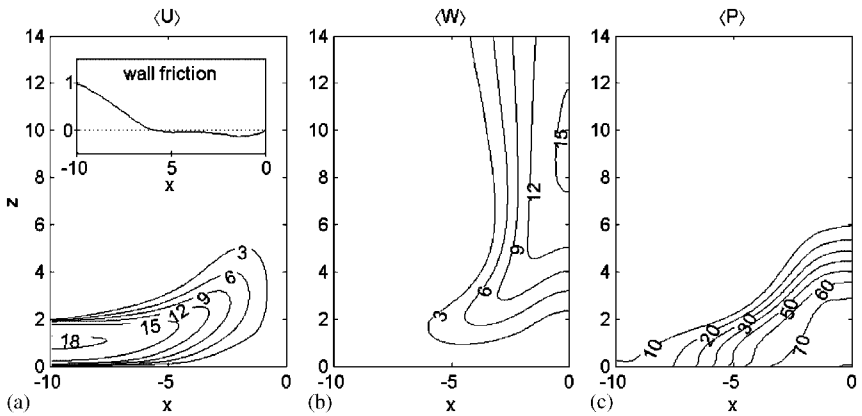

Figure 3. Mean velocity in x- and z-direction and mean pressure, $\langle U \rangle$, $\langle W \rangle$ and $\langle P \rangle$.

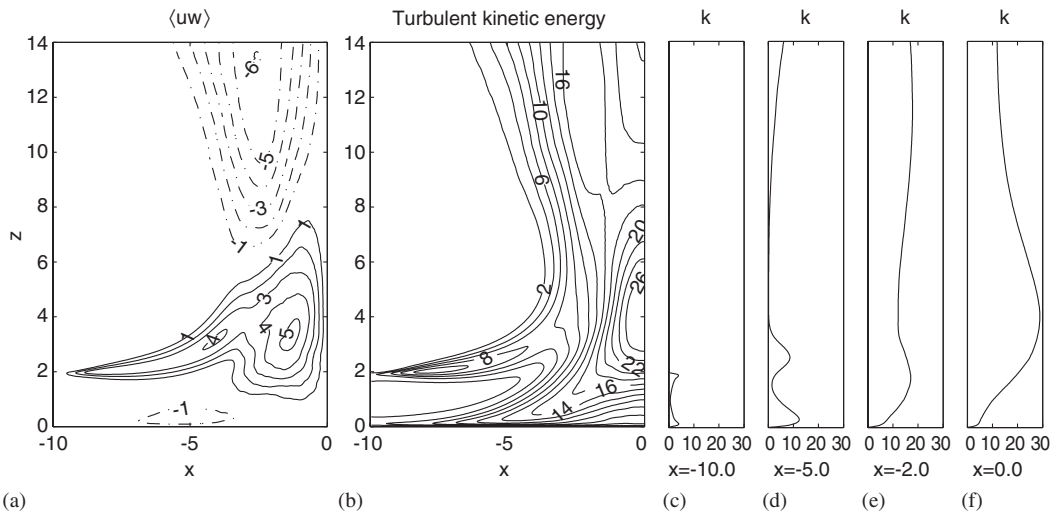

Figure 4. Turbulent shear-stress and turbulent kinetic energy, $\langle uw \rangle$ and k.

approximately $x \approx -6$, a separation bubble is formed in the stagnation region. The single outwash jet shows indication of a linear growth rate before it leaves the domain, although the development section is too short to verify a similarity solution.

Figure 4(a) and (b) report the turbulent shear-stress and the turbulent kinetic energy. The U velocity entering the domain has strong shear both towards the wall and at $z = 2$. Around $z = 2$, the growth of the shear-stress correlation $\langle uw \rangle$ and turbulence production become considerably larger than towards the wall where the wall-normal component is blocked. In the stagnation region, the positive $\partial \langle W \rangle / \partial z$ gradient gives negative production for the wall-normal Reynolds stress $\langle ww \rangle$. However, the positive production of $\langle uu \rangle$ is larger, assuring a positive production of k. Negative production in some components might indicate that at least

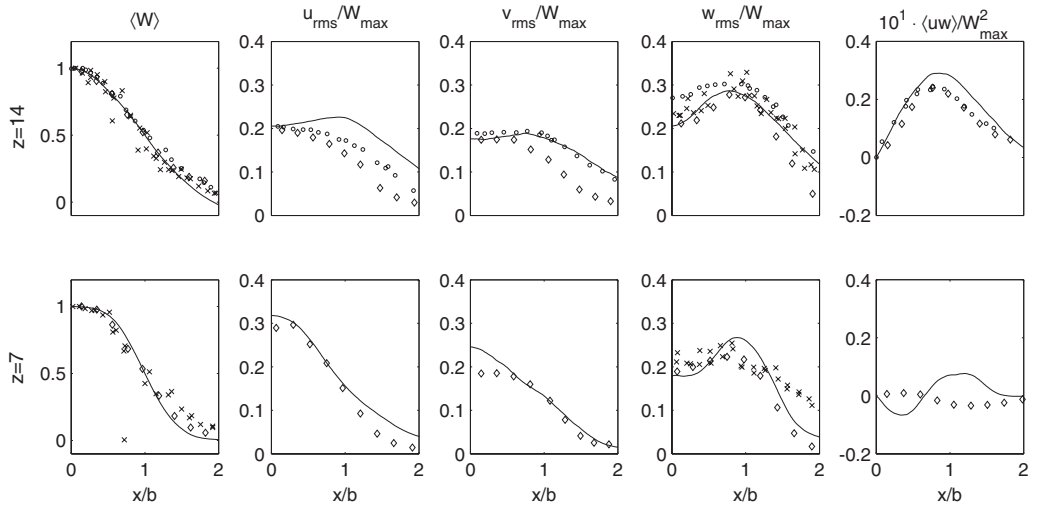

Figure 5. Mean velocity $\langle W \rangle$, turbulent shear-stress $\langle uw \rangle$ and rms-profiles in various cross sections of the merged jet. — DNS current study, ○ [6], ◇ [5], × [4].

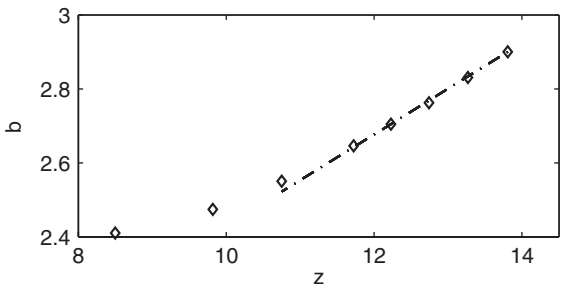

Figure 6. Growth of merged jet half width b as a function of z.

k–ε turbulence models may overestimate the turbulence level since they only predict positive production. Further up in the outwash jet the typical shear-stress profile of a planar jet is seen.

In Figure 4(c)–(f) profiles of k are shown at 4 different x positions. At $x = -10$ the typical channel flow profile is seen. The turbulence energy rapidly increases towards the merged jet's centreline at $x = 0$, where the maximum kinetic energy appears at $z \approx 4$. The increase in maximum energy level is about 500% compared to the maximum level in the channel profile and the turbulence intensity ($= \sqrt{k}/W$) is about 60%. The rapid increase in turbulence energy shows that the production mechanisms are present in the inlet turbulence. If not realistic turbulence is given as boundary conditions, the energy has a tendency to decrease before the turbulence reorganizes, becomes self-sustained and can start to grow again (see Figure 2 and also References [7, 8]).

Figure 5 shows mean velocity $\langle W \rangle$, rms-profiles and turbulent shear-stress $\langle uw \rangle$ of the merged jet. The results are compared with experimental data from two opposing curved wall

jets [5] and two opposing plane wall jets [4]. Considering the dissimilarities of the colliding flows, the level of turbulence intensities after interaction is remarkably similar. However, significant deviations are present in the turbulent shear-stress at $z = 7$. At $z = 14$, the turbulence intensities of the DNS have the same magnitude as the intensities of the self-similar plane jet [6]. Figure 6 shows b as a function of z. Here, b is the x position where the merged jet mean velocity $\langle W \rangle$ is half the centreline velocity. The growth rate $\mathrm{d}b/\mathrm{d}z$ is found to be 0.125, which is less than the value of 0.15 reported in Reference [5] and the value of approximately 0.2 found in Reference [4]. The reason might be that the boundary conditions used here are very regular such that flapping of the jet is not easily triggered.

In this study, reduced basis simulations are used to generate boundary conditions corresponding to turbulent plane channel flow. However, we believe that the method, with some manipulation of the channel POD modes, can be used for generating boundary conditions for a turbulent boundary layer as well.

REFERENCES

1. Saripalli KR. Laser doppler velocimeter measurements in 3-d impinging twin-jet fountain flows. *Turbulent Shear Flows 5*. Springer: Berlin, 1987; 146–168.
2. Zhao Y, Brodkey RS. Averaged and time-resolved, full-field (three-dimensional), measurements of unsteady opposed jets. *Canadian Journal of Chemical Engineering* 1998; **76**:536–545.
3. Behnia M, Parneix S, Durbin PA. Prediction of heat transfer in an axisymmetric turbulent jet impinging on a flat plate. *International Journal of Heat and Mass Transfer* 1998; **41**:1845–1855.
4. Gilbert BL. Turbulence measurements in a two-dimensional upwash. *AIAA Journal* 1988; **26**:10–14.
5. Park SO, Rew HS. Turbulence measurements in a merged jet from two opposing curved wall jets. *Experiments in Fluids* 1991; **10**:241–250.
6. Gutmark E, Wygnanski I. The planar turbulent jet. *Journal of Fluid Mechanics* 1976; **73**:465–495.
7. Holdø AE, Simpson BA. Simulations of high-aspect-ratio jets. *International Journal for Numerical Methods in Fluids* 2002; **39**:343–359.
8. Klein M, Sadiki A, Janicka J. Influence of the boundary conditions on the direct numerical simulation of a plane turbulent jet. *Proceedings of the 3rd International Symposium on Turbulence and Shear Flow Phenomena*, vol. 1, Stockholm, 2001; 401–406.
9. Johansson PS, Andersson HI. Generation of inflow data for inhomogeneous turbulence. *Theoretical and Computational Fluid Dynamics* 2004; **18**:371–389.
10. Lumley JL. *Stochastic Tools in Turbulence*. Academic Press: New York, 1970.
11. Sirovich L, Ball KS, Handler RA. Propagating structures in wall-bounded turbulent flows. *Theoretical and Computational Fluid Dynamics* 1991; **2**:307–317.
12. Johansson PS, Andersson HI, Rønquist EM. Reduced-basis modeling of turbulent plane channel flow. *Computers and Fluids* 2005, in press.
13. Manhart M. A zonal grid algorithm for dns of turbulent boundary layers. *Computers and Fluids* 2004; **33**: 435–461.
14. Pauley LL, Moin P, Reynolds WC. A numerical study of unsteady laminar boundary layer separation. *Report TF-34*, Thermosciences Division, Department of Mechanical Engineering, Stanford University, 1988.

